Article:
Mussatayev, M., Kempka, R., Tomlinson, K. et al. (2026) High-speed eddy current testing in ensuring rail integrity: an inspection-based study. Engineering Research Express, 8 (5). 055503. ISSN: 2631-8695

https://doi.org/10.1088/2631-8695/ae484e

PAPER • **OPEN ACCESS**

High-speed eddy current testing in ensuring rail integrity: an inspection-based study

To cite this article: Meirbek Mussatayev *et al* 2026 *Eng. Res. Express* **8** 055503

Engineering Research Express

OPEN ACCESS

RECEIVED
26 November 2025

REVISED
15 December 2025

ACCEPTED FOR PUBLICATION
19 February 2026

PUBLISHED
5 March 2026

PAPER

High-speed eddy current testing in ensuring rail integrity: an inspection-based study

Meirbek Mussatayev[1,2,3,*], Ruby Kempka[4], Kate Tomlinson[4], Roger Lewis[4], Nurdos Omarkulov[3], Gulsim Rysbayeva[3,5], Manat Tuenbayev[3] and Oluwatamilore A Adenipekun[4]

[1] School of Electrical, Electronic and Mechanical Engineering, University of Bristol, Bristol, BS8 1TR, United Kingdom
[2] Kazakhstan Institute of Non-Destructive Evaluation LLP, Astana, Z10H9C3, Kazakhstan
[3] Mukhametzhan Tynyshbaev ALT University, 97, Shevchenko str., Almaty, A05K3F6, Kazakhstan
[4] School of Mechanical, Aerospace and Civil Engineering, University of Sheffield, Sheffield, S1 3JD, United Kingdom
[5] School of Information Technologies and Applied Mathematics, SITAM, SDU University, 1/1 Abylai Khan, Kaskelen, 040900, Kazakhstan
[*] Author to whom any correspondence should be addressed.

E-mail: Meirbek.Mussatayev@bristol.ac.uk **and** m.musataev@alt.edu.kz

Keywords: Eddy current testing, high-speed inspection, rail integrity, non-destructive testing

Abstract

A new directional Eddy Current Probe has been developed and previously tested statically on typical rail damage types. To better understand its damage detection capability, knowledge of its performance while being moved along a track section was required as well as application to a wider range of potential rail flaws. High-speed stud inspections were conducted using damaged rail extracted from the field at velocities up to 2 m s^{-1} to evaluate the probe's reliability for potential deployment on a hand-pushed trolley. The inspection of rail studs at 2 m s^{-1} achieved an signal-to-noise ratio of 3.5, exceeding the industry-accepted threshold of 3.0. This result confirms the system's robust defect detection performance under dynamic operating conditions. The current field-representative set-up maintained reliable defect detectability across all tested speeds. These findings underscore the probe's operational resilience and validate its applicability for real- world rail maintenance scenarios where mechanical constraints and environmental variability are unavoidable.

1. Introduction

Railways remain a vital mode of freight and passenger transportation worldwide. For instance, in China alone, the national railway system serves tens of millions of passengers and transports over 50 million tonnes of freight annually, despite significant advancements in alternative transport systems [1]. Transcontinental initiatives such as the New Silk Road Railway [2] not only facilitate international trade but also underscore the critical need for resilient and reliable infrastructure. Ensuring the structural integrity and operational safety of railway systems has therefore become a strategic priority. However, detecting rail defects remains a significant challenge due to the large volume of data generated and the complexity of isolating relevant signal segments for analysis. As a result, the development of intelligent, automated, and efficient defect detection systems is essential for enhancing train safety and enabling timely identification of track anomalies [3].

NDT is crucial for assessing the integrity of aging infrastructures. By identifying invisible flaws early, NDT ensures the safety of engineering structures and facilitates timely maintenance activities. Among electro-magnetic NDT methods, Eddy Current Testing (ECT) is the most popular. ECT is well-established, non-contact, high-speed, adaptable to harsh environments, and an ideal candidate for real-time inspection. It supports rapid scanning and the data it generates is inherently quantitative and requires minimal computational effort for post-analysis [4]. Despite its many advantages, ECT has limited penetration depth when applied to high-density rail steel-typically only a few millimeters from the surface-due to its electromagnetic operating principle. Consequently, several studies [5–7] have highlighted its role as a complementary technique to ultrasonic testing (UT), which is more effective for deeper subsurface evaluation. However, the widely used Ultrasonic

(UT) NDT cannot detect studs, a squat-type RCF defect, in rails smaller than 4 mm in depth during high-speed (above 15 km h^{-1}) inspections [8]. This constraint reduces its effectiveness for identifying early-stage surface damage or fatigue cracks on the rail head. Given its sensitivity to surface-level anomalies, ECT is particularly well-suited for detecting localized damage such as cracks, corrosion, or wear on the rail head. A previous study [3] was conducted to identify optimal configurations for transmit and differential receive (Tx-dRx) ECT sensors, focusing on maximizing the Signal-to-Noise Ratio (SNR). The findings indicated that an ECT probe equipped with figure-8-shaped excitation coils paired with rectangular receiver can effectively detect the types of defects examined in this research, yielding a relatively high SNR. Robustness beyond studs was demonstrated in our prior work [9], where the same directional ECT architecture consistently detected rolling contact fatigue cracks and squats with SNRs $\geqslant$ 3–5, depending on spacing and surface roughness. Sensitivity remained above 5 at lift-offs up to 10mm (SNR $>$ 18 at 2 mm), confirming resilience to vibration-induced variations typical of in-motion inspections.

Recent advancements in NDT have significantly improved the detection of high-density rail defects, particularly under dynamic and industrial conditions. A growing body of research has focused on developing intelligent, contactless, and high-resolution systems tailored to the complex geometries and operational environments of railway infrastructure.

Mei *et al* [10] introduced a vision-based system for high-speed train body inspection that leverages a Siamese Transformer architecture to address challenges such as lighting variability, contamination, and structural complexity. By enabling comparative image analysis, the system effectively identifies surface-level anomalies, including foreign object attachments and component loosening, with a mean Intersection over Union of up to 86.29%. However, its lack of depth resolution limits its applicability for subsurface defect detection.

To overcome this limitation, Zhang *et al* [11] developed a robotic Ultrasonic Testing (UT) system for wheel inspection in noisy industrial environments with limited defect sample availability. Operating in pulse-echo mode at 3.5–5 MHz, the system employs both phased array and conventional probes to acquire A-scan and B-scan data during wheel rotation. Detection reliability is enhanced through synthetic data augmentation and YOLO-based object detection, enabling robust identification of buried defects such as hub cracks and rim fatigue zones.

Building on UT methodologies, Appiani *et al* [12] proposed an Electromagnetic Acoustic Transducer (EMAT)-based UT system for rail foot inspection. Designed to mitigate coupling variability, lift-off effects, and restricted access in dynamic settings, the system operates in pulse-echo mode using shear vertical bulk waves at central frequencies of 1889–2266 kHz. It successfully detected semi-elliptical flaws up to 10 mm deep, with quantitative validation via signal feature extraction and probability of detection (POD) modeling during bogie-mounted in-motion tests.

Complementing these UT approaches, Zhou *et al* [13] developed a non-contact ECT system for fatigue crack detection in high-speed railway contact wires. Tailored for high-altitude and high-voltage environments where manual inspection is impractical, the system utilizes a 30 kHz excitation coil and maintains a 0.5 mm lift-off distance. Voltage signal analysis and feature extraction, combined with neural network classification, yield 100% accuracy in crack width detection and 85.71% in depth estimation for defects ranging from 0.1 to 0.7 mm.

Miles *et al* [14] further advanced hybrid NDT approaches by combining EMATs with motion-induced eddy current (MIEC) sensing for in-motion detection of rolling contact fatigue (RCF) damage. EMATs operating at 1 MHz detect subsurface flaws up to 4.5 mm deep, while the MIEC module-based on Hall-effect sensors–enhanced sensitivity to surface-breaking defects. Hilbert transform envelope extraction and spatial probability density functions facilitated precise defect localization, achieving classification accuracy within 1% of physical measurements.

Induction thermography has also emerged as a promising non-contact technique. D'Accardi *et al* [15] investigated its application for rail flaw detection at inspection speeds up to 20 km h^{-1}. The study employed high-frequency induction heating (150–400 kHz) to generate thermal contrast through Joule heating and the skin effect, enabling crack visualization. Image processing methods such as scan-line reconstruction and Sobel edge detection enable the identification of sub-millimeter surface openings and buried defects, supporting its integration into diagnostic rail vehicles.

In addition, Wang *et al* [16] developed an ECT mapping system for evaluating laser-hardened 45 and 30Cr steel surfaces. Addressing the challenge of non-destructively assessing mechanical property variations induced by rapid thermal processing, the system scans hardened regions to detect electromagnetic response changes correlated with residual stress and surface hardness. Experimental results confirmed its effectiveness in differentiating hardened zones and characterizing stress distribution, making it suitable for high-speed, contactless quality assessment.

ECT, with its high sensitivity to surface defects and non-contact operation, has proven effective for evaluating such repairs. These insights support the use of ECT in post-cladding inspections to ensure early defect

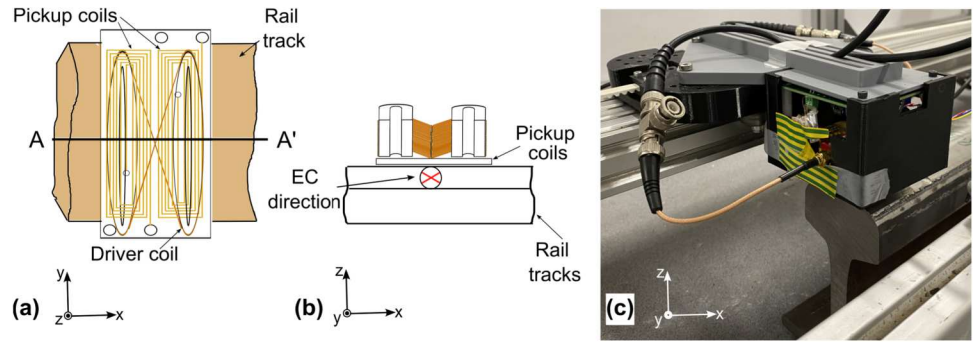

Figure 1. Schematic illustration of the key components of the ECT probe, comprising: (a) a top-down view of the probe positioned on the rail specimen; (b) a cross-sectional view along A-A′ detailing the proposed internal configuration; and (c) a photograph of the fabricated probe. Parts (a) and (b): Reproduced from [3]. CC BY 4.0.

detection and structural integrity. Furthermore, recent literature on local damage detection in high-speed rail infrastructure, such as the review by Wang *et al* [1], emphasizes the integration of stud detection into intelligent rail assessment platforms These systems increasingly incorporate advanced NDT modalities, including machine vision, UT guided waves, and ECT, to enhance the accuracy and reliability of defect identification and classification under dynamic operating conditions.

The objective of this study was to evaluate the performance of a directional ECT probe through controlled experimental trials on a representative stud defect in an extracted rail segment. The probe, engineered for integration with a mobile inspection trolley, was assessed for its effectiveness in detecting typical rail surface anomalies at inspection speeds of up to 2 m s^{-1}.

2. Establishing the inspection methodology based on eddy current testing

The methodology of this study builds upon prior investigations aimed at optimizing three ECT sensor configurations for detecting both artificially induced and naturally occurring defects in rail specimens, with the goal of identifying the most suitable configuration for integration into a hand-pushed device for real-time rail maintenance monitoring [3]. Subsequent work [17] evaluated the selected sensor under dynamic conditions, including inspection speeds of up to 1m s^{-1}. The developed probe was mobilized using the external composite cutter device Eagle-S125; however, this set-up does not fully replicate real-world inspection conditions. In practical scenarios, factors such as mechanical vibration and process-induced disturbances may adversely affect signal stability and reduce the achievable sensitivity, which reached up to 4.5 SNR at a scanning speed of 1 m s^{-1} under controlled conditions, as reported in [17]. Findings from these preliminary studies informed the design of further experiments involving higher velocities (up to 2m s^{-1}) and broader vibration profiles. For this purpose, a high-speed inspection rig was developed to simulate realistic NDT scenarios and to advance the technology readiness level of the proposed system.

2.1. Measurement mechanism

The operational principle of the proposed ECT probe is grounded in Faraday's law of electromagnetic induction. When an alternating current flows through the transmitter coil, it generates a time-varying magnetic field around the coil windings. This fluctuating field induces circulating eddy currents in any nearby electrically conductive and magnetically permeable material. These induced eddy currents, in turn, produce a secondary magnetic field that opposes the primary field. The characteristics of this secondary field, such as its strength and distribution, encode information about the local electrical conductivity and magnetic permeability of the specimen under inspection.

In the absence of defects, the eddy current flow remains undisturbed, resulting in a stable impedance profile across the receiver coil. However, the presence of discontinuities such as surface-breaking cracks disrupts the eddy current path, leading to localized changes in impedance. By monitoring voltage variations across the receiver coil, such anomalies can be detected and spatially resolved.

To support this mechanism, figure 1 illustrates the main components of the ECT probe: (a) a top-down view of the probe positioned on the rail specimen; (b) a cross-sectional view along A-A′ highlighting the internal design; and (c) a photograph of the fabricated probe. The material specifications and geometric parameters of the transmitter (Tx) and receiver (Rx) coils used in the experimental setup are detailed in table 1.

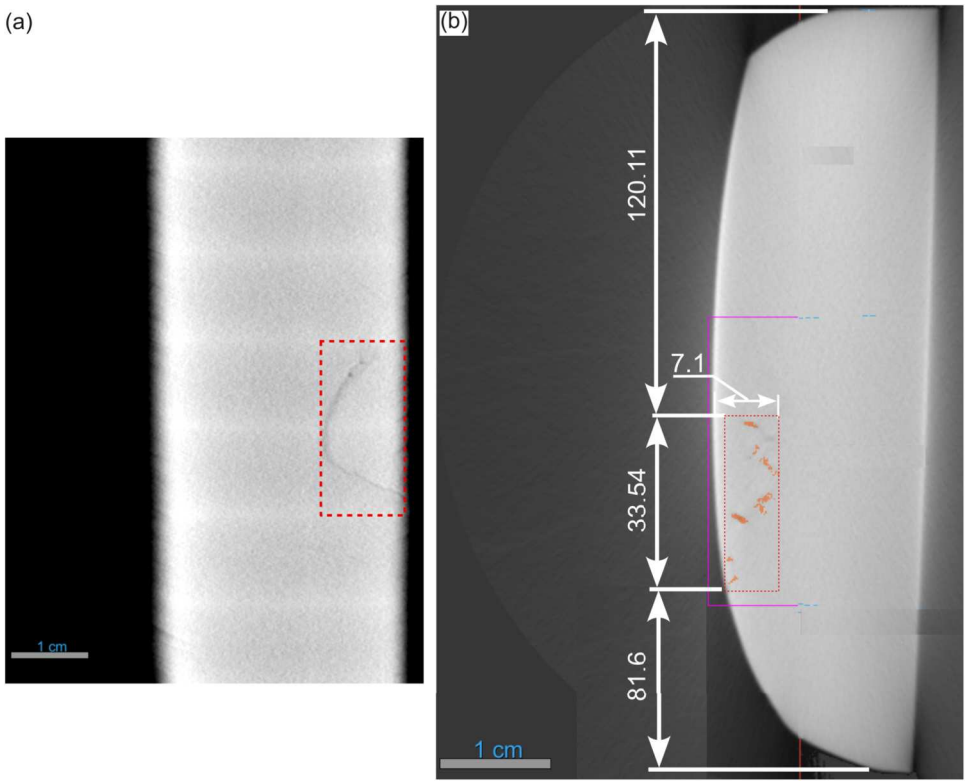

Figure 2. Specimen under inspection: (a) top-view μ-CT image captured at a depth of 1.15 mm from the rail head surface; (b) cross-sectional side-view μ-CT scan of the rail sample with a stud, illustrating stud positions and the spatial extent of the affected zone. Reproduced from [9]. CC BY 4.0.

Table 1. Material specifications and geometric parameters of Tx and Rx coils.

Coil Type	Material	Turns	Size (mm)	Inductance (μH)
Tx coil pair	Copper, Ø0.2 mm	24	158	60.8
Rx coils	FR4 substrate	12	30 × 7.5	2.64

Building upon the foundational study conducted by Mussatayev *et al* [4], this work employs signal-to-noise ratio (SNR) analysis to rigorously evaluate the probe's performance across a range of inspection conditions, as defined in the equation below. The acceptance threshold of SNR $\geqslant 3$ is consistent with established standards and reported practices in nondestructive evaluation. For example, the Department of Defense Military Handbook [18] defines a minimum SNR of 3 for reliable defect detection. This threshold is further supported by Hughes and Dixon's performance analysis of single-frequency near electrical resonance signal enhancement (SF-NERSE) techniques [19], where SNR $\geqslant 3$ was used as a benchmark for signal reliability in defect characterization. The SNR is computed using equation (1):

$$\mathrm{SNR} = \frac{V_{\max} + |V_{\min}|}{2 \cdot \mathrm{RMS}(N)} \tag{1}$$

where, $V_{\max}$ and $V_{\min}$ correspond to the maximum and minimum voltage amplitudes observed within the defect region, and RMS(N) denotes the root-mean-square value of the signal acquired from non-defective areas, serving as a baseline noise reference.

2.2. Materials under inspection

To evaluate performance under dynamic conditions, an additional specimen with 235 × 75 × 20 mm dimensions, featuring studs was prepared for high-speed inspection trials. Figure 2 presents both damaged configurations, along with their respective dimensional specifications. Metallurgical analysis of the molten rail substrate revealed a carbon concentration ranging from 0.87% to 0.97% by weight, consistent with medium-carbon steel compositions used in rail infrastructure.

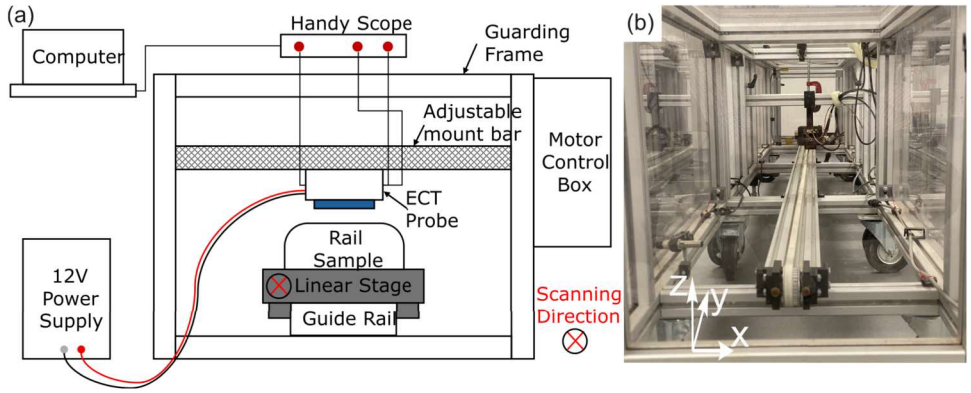

Figure 3. Measurement setup for high-speed eddy current inspection: (a) schematic diagram of the ECT configuration integrated into the inspection rig; (b) photograph of the developed rail-based inspection system.

2.3. Experimental set-up

To experimentally validate the proposed mechanism, a high-speed linear actuator rig equipped with compact ECT instrumentation was utilised as shown in figure 3(a). The linear actuator rig consists of a 3 m belt-driven linear stage powered by a 3 Nm stepper motor with a NEMA 23 size faceplate. The actuator is housed within an aluminium extrusion frame, which is enclosed with polymethyl methacrylate panels for safety. The motor driver and power supply are integrated into a dedicated control box. The actuator accelerates linearly to a predefined speed with a set acceleration and subsequently decelerates to a stop. Its operating speed range spans from 0.2 m s^{-1} to 4 m s^{-1}. The ECT probe is mounted on an adjustable support bar, enabling vertical height adjustment of the gap between the ECT sensor and the rail sample. For the ECT measurement process, a 0.3 MHz sinusoidal excitation signal with 1 Vpp amplitude was generated using the Handyscope HS5 (TiePie Engineering, The Netherlands) and fed into the voltage input of a Howland current source board located within the probe housing. This source delivered a stable current to the Tx coil, producing a primary magnetic field. When the rail specimen was positioned in proximity, it induced eddy currents within the material, which in turn generated a secondary magnetic field opposing the primary one. This secondary field encodes information about the local electrical conductivity and magnetic permeability of the scanned region.

Defect detection was achieved by observing impedance variations in the receiving coil. A differential ECT probe, mounted $\approx$ 2 mm above the rail surface, was connected to the detection unit. The rail sample was linearly translated beneath the probe at speeds ranging from 0.2 to 2.0 m s^{-1} in 0.2 m s^{-1} increments, while the probe remained stationary during data acquisition. The differential voltage signal from the pickup coil was routed back to the Handyscope, where it was compared in real time with the reference voltage from the current source using MATLAB on a connected laptop. A $\pm$12 V DC power supply was used to energize the differential amplifier. The actual photo of experimental setup is shown in figure 3(b).

Figure 4 presents the sensor signal acquired during high-speed inspection. Initially, from 0 to 9 seconds, the probe recorded baseline noise while scanning through air. A distinct negative voltage peak marked the onset of rail material detection. Once the probe passed over the conductive surface, the mean voltage signal dropped below the air baseline, indicating material interaction. Between 13.5 and 15 seconds, a localized signal disturbance, highlighted by vertical dashed lines, corresponded to the presence of studs, with sufficient signal length to define a failure event (see figure 4). The regions flanking the defect zone were used to estimate background structural noise for SNR calculation, as defined in equation (1). A subsequent positive peak indicated the end of the material scan. The remainder of the time trace reflects probe behavior in air, and the total measurement duration was truncated to emphasize the relevant signal segment.

3. Measurement results

This section presents a performance evaluation of the directional ECT probe during the inspection of a studded rail specimen, conducted using a high-speed scanning rig designed to simulate field-representative conditions. The probe, previously optimized for frequency selection and lift-off variation in earlier studies by the authors, is applied here without further modification, utilizing the established parameters for performance assessment.

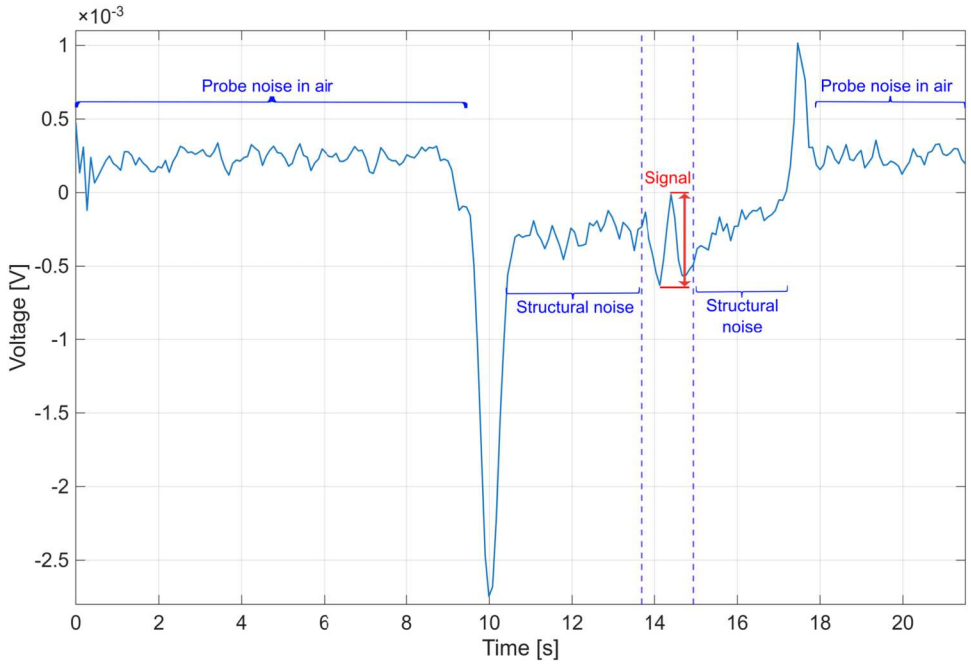

Figure 4. Exemplar plot of high-speed sensor signals at 0.2 m s^{-1}.

3.1. High-speed sensor signals

A sensitivity assessment of the ECT probe was conducted using a precision-controlled, high-speed scanning rig. In this configuration, the rail specimen was translated along a linear axis while the probe remained fixed in position, ensuring consistent spatial alignment throughout the inspection. Sample movement was governed by an external motion controller, whereas the data acquisition and inspection logic were implemented within a MATLAB-based control environment, enabling synchronized triggering and signal capture.

Figure 5 presents representative ECT signal waveforms acquired at various scanning velocities. Across all tested speeds, the probe demonstrated robust defect detection capability, as evidenced by the pronounced and symmetric signal profiles. This symmetry is characteristic of the differential winding configuration of the receiver coil, which enhances sensitivity to localized impedance variations.

At scanning velocities exceeding 1 m s^{-1}, a marked reduction in the number of impedance data points per measurement was observed, indicating diminished temporal resolution under high-speed conditions. This limitation is attributed to the constrained computational throughput of the real-time post-processing pipeline, compounded by the analog nature of the prototype current source and amplifier circuitry. These hardware constraints restrict the temporal resolution of impedance sampling during high-speed motion.

To address these limitations, future iterations of the system will incorporate enhanced digital signal processing modules, optimized firmware routines, and upgraded analog front-end components. These improvements aim to increase data acquisition density and maintain signal fidelity under dynamic inspection conditions.

3.2. Comparative evaluation of ECT probe sensitivity across two studies

To quantitatively assess the probe's performance, SNR metrics were computed using three independent repetitions of the ECT scan data. As illustrated in figure 6, the targeted defect was reliably detected across each speed, with SNR values consistently exceeding 2.5. This confirms the probe's suitability for high-resolution defect characterization under varying operational speeds.

Both the previous investigation [17] and the present study employed identical ECT instrumentation, probe architecture, and rail-grade material to ensure methodological consistency and facilitate reproducibility. This deliberate alignment of experimental parameters enables a robust comparative analysis of probe sensitivity across varying operational contexts. Notably, the earlier study [17] was conducted under controlled laboratory conditions using an external high-speed simulation device, thereby minimizing extraneous variability. In contrast, the current study was designed to emulate a field-representative industrial environment, incorporating realistic mechanical constraints and ambient influences that more accurately reflect in-service inspection scenarios.

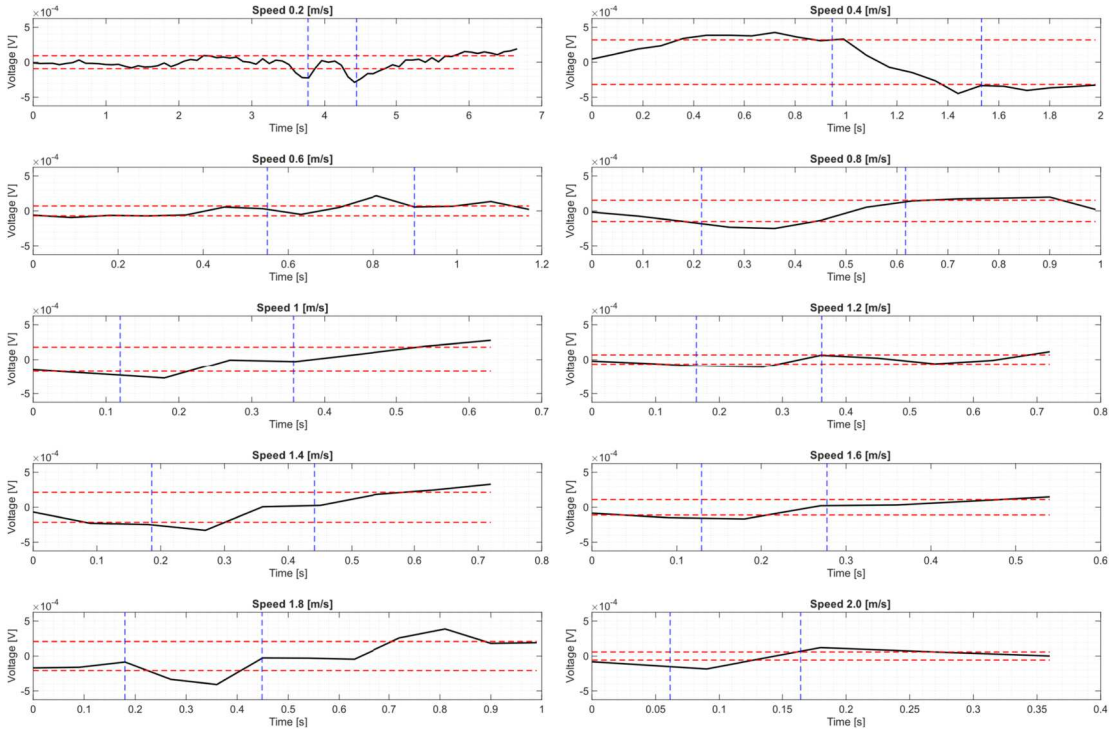

Figure 5. Representative high-speed ECT sensor signals acquired at scan velocities ranging from 0.2 m s^{-1} to 2.0 m s^{-1} in 0.2 m s^{-1} increments.

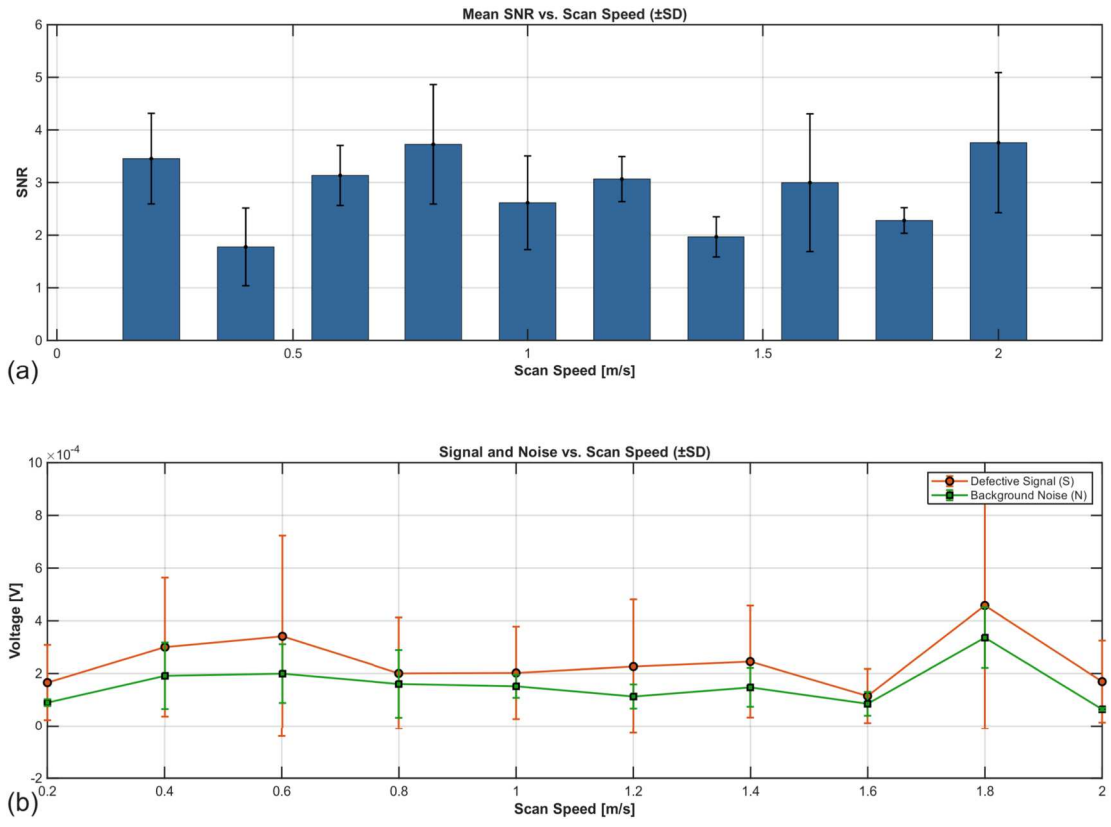

Figure 6. High-speed ECT probe evaluation at scan velocities up to 2 m s^{-1}, with results averaged over three repeated scans and corresponding error bars: (a) histogram of estimated SNR values; (b) signal and structural noise contributions plotted for each inspection speed.

Table 2. Maximum SNR comparison between study 1 and study 2 at selected speeds.

Speed (m s^{-1})	Previous study [17]	Current study
0.2	6.78	4.39
0.4	6.81	2.63
0.8	6.76	5
1.0	6.76	3.17

SNR values were computed using the standardized formulation (see equation (1)) and averaged over three independent scans per velocity setting. To ensure statistical and methodological validity, only matching scan velocities–specifically 0.2, 0.4, 0.8, and 1.0 m s^{-1}–were selected for direct comparison. The resulting maximum SNR values from both studies are summarized in table 2.

4. Discussion

Beyond the incremental speed increase, this study demonstrates a single-modality directional ECT probe that remains robust under field-representative mechanical and environmental constraints, thereby advancing its readiness for routine rail maintenance. In contrast to Zhou *et al* [13], whose neural-network approach to contact wire cracks relied on large datasets, and Miles *et al* [14], whose hybrid EMAT–ECT system added complexity and cost, the present probe achieves reliable stud detection with a simpler physics-based architecture, consistently maintaining SNR $\geqslant$ 3 across dynamic rail head inspections. Thus, by emphasizing simplicity, reproducibility, and deployability, the system complements established NDT methods–surpassing EMAT-UT in shallow stud detection and offering a lower-cost alternative to induction thermography–while providing a practical solution for lightweight trolley integration in real-world rail monitoring. A comparative analysis of the proposed directional ECT probe and recent approaches by [14] and [13], highlighting key differences in design, resilience, processing, defect sensitivity, and overall improvements, is presented in table 3.

Further comparative analysis of how the proposed ECT probe outperforms or complements EMAT-based UT [12] and induction thermography [15] in real-world deployment is summarized in table 4. In real-world deployment, the proposed directional ECT probe offers clear advantages over EMAT-UT [12] and induction thermography [15]. It provides higher sensitivity to shallow, surface-critical defects such as studs and head checks at practical trolley speeds and lift-offs, while requiring simpler and lower-cost hardware. Unlike UT or thermography, ECT avoids coupling and emissivity constraints, ensuring robust SNR and repeatable detection under dynamic conditions. EMAT-UT remains valuable for subsurface rail foot and web defects, and induction thermography excels in full-field imaging at higher speeds. Together, these methods form a complementary diagnostic stack–ECT for surface anomalies, IRT for near-surface coverage, and EMAT-UT for volumetric inspection–enabling comprehensive rail integrity assessment with improved confidence in defect detection.

The proposed directional ECT probe demonstrates reliable defect detection capabilities but faces computational limitations due to MATLAB-based signal processing, which introduces 50–100 ms processing delays unsuitable for high-speed applications above 2 m s^{-1}. Current analog circuitry and sequential processing architecture restrict real-time performance, limiting temporal resolution and data acquisition density at elevated scanning speeds. The current MATLAB-based visualization system experiences refresh delays that compromise real-time monitoring capabilities at high speeds.

To overcome these constraints, future system iterations will transition from MATLAB to optimized C++ software implementation utilizing dedicated DSP libraries (FFTW3, Eigen3) and multi-threaded architecture (see figure 7(a)). Figure 7(b) shows the display interface where time trace plots will be displayed in real-time, enabling operators to visualize voltage variations, impedance changes, and defect signatures during continuous scanning operations. The upgraded software framework will feature enhanced time trace visualization with sub-millisecond refresh rates, supporting real-time signal plotting, automated defect marking, and synchronized data logging. This software migration is expected to reduce processing time to sub-millisecond levels while providing smooth, responsive time trace displays that enable inspection speeds of 5–10 m s^{-1}. The new C++ interface will maintain signal fidelity during dynamic visualization and enhance deployment flexibility through elimination of MATLAB runtime dependencies, making the system suitable for field deployment and commercial rail monitoring applications. Beyond code optimization, the study introduces adaptive filtering, multi-scale windowing, and envelope-based feature fusion to stabilize SNR and improve defect localization at high speeds, representing a methodological advance in ECT data processing.

Across all comparable speeds, the first study consistently yielded higher peak SNRs, with the most pronounced difference observed at 0.4 m s^{-1} (6.81 versus 2.63) (see table 2). These findings suggest that while the

Table 3. Comparative analysis of the proposed directional ECT probe against recent state-of-the-art approaches by Miles *et al* [14] and Zhou *et al* [13].

Probe Architecture and Simplicity	Operational Resilience in Field-Representative Conditions	Data Processing and Deployment Efficiency	Defect Class Sensitivity	Summary of Fundamental Improvements
Single-modality directional ECT with streamlined coils; avoids hybrid or AI complexity.	Stable under vibration and noise; reliable detection at 2 m s^{-1}.	Direct SNR analysis; real-time detection without heavy computation.	Sensitive to shallow studs ($<$ 4 mm) often missed by UT/EMAT.	Low-cost, reproducible, and field-ready for routine monitoring.
[14]: hybrid EMAT-MIEC probe with complex dual modules.	Tested mainly at low speeds; lacks field realism.	Requires multi-modal fusion; adds latency.	Detects deeper RCF cracks; shallow studs remain difficult.	Less deployable; higher cost and footprint.
[13]: neural-network ECT for contact wires; dataset-dependent.	Focused on static/low-speed wires; not rail studs.	Needs BP neural networks; offline training required.	Effective for wire cracks (0.1–0.7 mm), not rail squats.	Adds AI overhead; ECT here offers lightweight alternative.

Table 4. Comparative analysis of rail NDT methods highlighting detection accuracy, speed, cost, defect applicability, limitations, and deployment readiness.

Method	Detection accuracy	Speed capability	Cost (relative)	Best-suited defect types	Key limitations / Readiness
Directional ECT [current work + [9]]	SNR up to 47 for studs; reliable for cracks/squats; lift-off tolerance to 10 mm.	Demonstrated up to 2 m s^{-1}; repeatable dynamic scans.	Low-moderate; compact, no coupling, simpler than EMAT/IRT.	Surface studs, squats, RCF cracks, weld anomalies.	Shallow focus; limited depth. Field-ready for trolley use, validated with μ-CT.
EMAT-based UT	POD Area90/95 172-410 mm^2; bogie tests 90% (high-freq) versus 77.5% (low-freq).	Bogie tests up to 7 km h^{-1}; lab scans 1-2 km h^{-1}.	Moderate-high; requires high-power drivers and magnets.	Subsurface/web/ foot flaws; broader RCF.	Lift-off sensitivity; shielding needed. Prototype proven, upgrades required for higher speeds.
Induction thermography	Robust crack contrast; early head checks detectable at 1 kW.	Demonstrated up to 20 km h^{-1} with scan-line/matrix reconstruction.	Moderate-high; cooled IR camera, induction source, mirrors.	Surface/near-surface cracks, head checks, squats.	Emissivity dependent; limited frames at speed. Strong lab feasibility, pairing with UT advised.

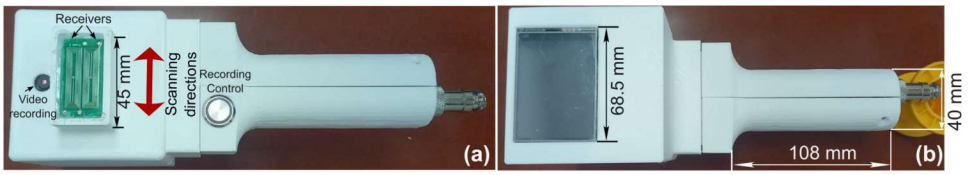

Figure 7. Prototype of a portable inspection device featuring integrated high-resolution video capture: (a) overview of the front interface layout; (b) physical dimensions.

laboratory-controlled setup may optimize signal clarity, the industrially constrained configuration introduces additional noise factors that attenuate probe sensitivity. Such insights are critical for calibrating ECT systems for real-world deployment, where environmental robustness must be balanced against diagnostic precision.

Importantly, both studies confirm the probe's operational integrity and defect detection potential up to 1.0 m s^{-1}, validating its suitability for high-throughput rail inspection. The comparative analysis underscores the importance of optimizing mechanical integration and signal conditioning for industrial deployment without compromising metrological reliability.

The developed ECT device demonstrates robust operational stability under challenging inspection conditions, including elevated scan speeds and environments characterized by mechanical vibration. These design enhancements aim to improve the probe's sensitivity to both surface-breaking and subsurface anomalies. A portable version of the probe has been further refined beyond its earlier iteration presented in [17], incorporating mechanical and electronic upgrades to support field deployment (see figure 7).

Although high-speed FPGA-based systems [20] have reported inspection velocities far beyond 2 m s^{-1}, the novelty of our work lies in demonstrating a directional ECT probe that maintains reliable stud detection under realistic trolley-based conditions. The probe achieved SNR $\geqslant$ 3.5 at 2 m s^{-1} while tolerating lift-off and vibration, confirming robustness in field-representative environments. Unlike algorithmic acceleration studies, our contribution emphasizes hardware simplicity, reproducibility, and deployability for routine rail maintenance. Thus, the proposed ECT system complements existing EMAT-UT and induction thermography approaches by providing a practical, low-cost solution for shallow surface defect detection in real-world scenarios.

5. Conclusions

This study validated the performance of a directional ECT probe for detecting high-speed stud inspections at velocities up to 2 m s^{-1} achieved peak SNR values of 3.7. These results confirm the probe's sensitivity to interface-related discontinuities and its operational reliability under realistic mechanical constraints. The successful detection of targeted flaws across all tested velocities supports the probe's suitability for hand-push deployment in field environments and its integration into high-speed rail maintenance workflows. The study in [9], together with current results, demonstrates that the directional ECT probe reliably characterizes diverse rail defects, with μ-CT validation for studs, stable detection of RCF cracks and squats, and dynamic stud detection at 2 m s^{-1} evidencing field readiness. Overall, the findings contribute to the advancement of NDT strategies for repaired rail infrastructure, particularly in scenarios involving dynamic inspection requirements.

Acknowledgments

This research has been/was/is funded by the Science Committee of the Ministry of Science and Higher Education of the Republic of Kazakhstan (Grant No. AP26102347). The authors express their gratitude to Dr Fernando Alvarez-Borges, Senior Research Fellow, μ-VIS x-ray Imaging Centre, University of Southampton, for his invaluable assistance in the interpretation of the x-ray CT validation results.

Data availability statement

The data that support the findings of this study are openly available at the following URL/DOI: https://doi.org/10.21227/eb4b-5072.

AI tools disclosure

The authors acknowledge Microsoft Copilot support for language refinement.

Declaration of competing interest

The authors declare no conflicts of interest.

Author contributions

Meirbek Mussatayev 0000-0001-9563-8805
Conceptualization (lead), Data curation (supporting), Investigation (lead), Methodology (lead), Resources (supporting), Software (equal), Visualization (equal), Writing – review & editing (equal)

Ruby Kempka
Data curation (equal), Resources (equal)

Kate Tomlinson 0000-0003-4691-5057
Project administration (equal), Resources (supporting)

Roger Lewis
Supervision (lead), Writing – review & editing (equal)

Nurdos Omarkulov
Software (equal)

Gulsim Rysbayeva 0000-0002-7331-353X
Formal analysis (equal), Project administration (equal), Visualization (equal)

Manat Tuenbayev
Resources (equal)

Oluwatamilore A Adenipekun
Resources (equal)

References

[1] Wang Y, Miao B, Zhang Y, Huang Z and Xu S 2025 Review on rail damage detection technologies for high-speed trains *Applied Sciences (Switzerland)* **15** 7725
[2] Fang L, Kleimann M, Li Y and Schmerer H-j 2021 The implications of the New Silk Road Railways on local development *Journal of Asian Economics* **75** 1–15
[3] Mussatayev M, Kempka R and Alanesi M 2024 Towards advancing real-time railroad inspection using a directional eddy current probe *Sensors* **24** 6702 https://www.mdpi.com/1424-8220/24/20/6702
[4] Mussatayev M, Yi Q, Fitzgerald M, Maes V K, Wilcox P and Hughes R 2024 Directional eddy current probe configuration for in-line detection of out-of-plane wrinkles *Composites Part B: Engineering* **268** 111048 https://linkinghub.elsevier.com/retrieve/pii/S1359836823005516
[5] Santos D, Machado M A, Monteiro J, Sousa J P, Proença C S, Crivellaro F S, Rosado L S and Santos T G 2023 Non-destructive inspection of high temperature piping combining ultrasound and eddy current testing *Sensors* **23** 3348
[6] Song H, Xiao Q, Wang G, Zhang J and Hu W 2023 A composite approach of electromagnetic acoustic transducer and eddy current for inner and outer corrosion defects detection *IEEE Trans. Instrum. Meas.* **72** 1–11
[7] Wang J, Wang N, Xu J, Cao Y, Cao Y and Huang P 2023 Composite detection method for subsurface defects in gas gathering station pipelines using eddy current and ultrasonic techniques *roceedings - 2023 China Automation Congress, CAC 2023* 2949–53
[8] Papaelias M P, Lugg M C, Roberts C and Davis C L 2009 High-speed inspection of rails using ACFM techniques *NDT and E Int.* **42** 328–35
[9] Mussatayev M, Kempka R, Tomlinson K, Lewis R, Smagulova D, Rysbayeva G, Tuenbayev M and Adenipekun O A 2026 Design and real-time sensitivity evaluation of directional eddy current probes on extracted rails *Measurement: Journal of the International Measurement Confederation* **259** 119611
[10] Mei S, Wang H, Diao Z, Zhang J, Shen H and Wen G 2025 STCD-Net: a novel change detection architecture for anomaly detection on high-speed train body in railway maintenance *IEEE Trans. Instrum. Meas.* **74** 1–13
[11] Zhang Q, Tian K, Zhang F, Li J, Yang K, Luo L, Gao X and Peng J 2025 DiffUT: diffusion-based augmentation for limited ultrasonic testing defects in high-speed rail *NDT and E Int.* **154** 103388
[12] Appiani A and Carboni M 2025 A feasibility study on in-service non-destructive inspection of railway rails by an ultrasonic technique based on travelling electromagnetic acoustic transducers *Railway Engineering Science* **33** 684–702
[13] Zhou X, Sun W, Zhang Z, Zhang J, Chen H and Li H 2024 Eddy current quantitative evaluation of high-speed railway contact wire cracks based on neural network *Railway Sciences* **3** 764–78
[14] Miles Z *et al* 2024 Hybrid multi-modal NDE sensing system for in-motion detection and localization of rolling contact fatigue damage in rails *NDT and E Int.* **147** 103209

[15] D'Accardi E, Dell'Avvocato G, Masciopinto G, Marinelli G, Fumarola G, Palumbo D and Galietti U 2025 Evaluation of typical rail defects by induction thermography: experimental results and procedure for data analysis during high-speed laboratory testing *Quantitative InfraRed Thermography Journal* **22** 173–94
[16] Wang N, He C F and Liu X C 2022 Eddy current mapping technology for residual stress and surface hardness evaluation in laser hardened steels *J. Phys. Conf. Ser.* **2198**
[17] Mussatayev M, Fakih M A, Fitzgerald M, Lewis R, Beisenbekov A, Rysbayeva G and Rysbayev B 2026 Advanced real-time rail monitoring system based on directional eddy current probe *NDT & E International* **157** 103532 https://linkinghub.elsevier.com/retrieve/pii/S0963869525002130
[18] Annis C 2009 Mil-hdbk-1823a nondestructive evaluation system reliability assessment *Department of Defense Handbook* (Wright-Patterson AFB)
[19] Hughes R R and Dixon S 2019 Performance analysis of single-frequency near electrical resonance signal enhancement (SF-NERSE) defect detection *NDT and E Int.* **102** 96–103
[20] Miao Y, Huo J, Liu Z, Gao Y and Wang C 2022 Fast Rail Defect Inspection Based on Half-Cycle Power Demodulation Method and FPGA Implementation *Journal of Beijing Institute of Technology* **31** 185–95